ADVANCING EARTH AND SPACE SCIENCES

JGR Atmospheres

RESEARCH ARTICLE
10.1029/2026JD046751

The Source of Arctic Precipitation in HadGEM3-GC5

J. K. Ridley[1,†], A. J. McLaren[2], L. C. Sime[2], and E. W. Blockley[1]

[1]Met Office, Exeter, UK, [2]British Antarctic Survey, Cambridge, UK

†Retired.

Key Points:

- Water tracers in a climate model show substantial seasonal variability in the sources of Arctic precipitation
- Under global warming and associated sea ice decline, the locally sourced fraction of Arctic precipitation increases
- The remote source of Arctic precipitation remains the dominant source throughout the global warming simulation

Correspondence to:
A. J. McLaren and E. W. Blockley,
aliren@bas.ac.uk;
ed.blockley@metoffice.gov.uk

Citation:
Ridley, J. K., McLaren, A. J., Sime, L. C., & Blockley, E. W. (2026). The source of Arctic precipitation in HadGEM3-GC5. *Journal of Geophysical Research: Atmospheres*, *131*, e2026JD046751. https://doi.org/10.1029/2026JD046751

Received 23 FEB 2026
Accepted 13 AUG 2026

Author Contributions:
Conceptualization: J. K. Ridley, A. J. McLaren, E. W. Blockley
Funding acquisition: L. C. Sime
Methodology: J. K. Ridley, A. J. McLaren
Resources: A. J. McLaren
Software: J. K. Ridley, A. J. McLaren
Supervision: L. C. Sime, E. W. Blockley
Visualization: J. K. Ridley, A. J. McLaren
Writing – original draft: J. K. Ridley, A. J. McLaren
Writing – review & editing: J. K. Ridley, A. J. McLaren, L. C. Sime, E. W. Blockley

Abstract Snow and rain are increasing in the Arctic. Climate model projections indicate a 50% increase in precipitation by the end of the century. This increase is driven by increased local evaporation following reduced sea ice coverage alongside enhanced global evaporation and transport into the Arctic. The relative contributions of these sources of Arctic precipitation are directly assessed using water tracers in the HadGEM3 climate model. An idealized warming simulation shows that, whilst remote sources dominate over local sources of Arctic precipitation in all seasons, the proportion of locally ocean-sourced precipitation increases from 15% at the start of the run to 38% at $4 \times CO_2$. Once the Arctic sea ice has been lost, the fraction of precipitation from local ocean sources stops increasing. For each season this state tends to correspond to the time when Arctic precipitation also switches from snow to rain-dominated. The increase in the fraction of precipitation sourced from the Arctic Ocean (locally sourced) occurs in all seasons, except summer. In summer, the precipitation over the Arctic Ocean is instead mostly sourced from land evapotranspiration. Our water tracer method also reveals that a significant amount of Arctic evaporation is exported by the atmosphere out of the Arctic. This highlights that both the import and export of water vapor must be considered when investigating Arctic hydrological changes. Individual precipitation events tend to have multiple evaporative sources, indicating some mixing of vapor. Remotely sourced precipitation tends to dominate the Arctic margins while local Arctic sources dominate the interior.

Plain Language Summary Global warming will increase global evaporation which can be transported as vapor to the Arctic. Alongside this, sea ice cover is declining in the Arctic, which allows for more evaporation from the newly open Arctic Ocean. However, the relative importance of changing sea ice versus global evaporation is unclear. We track water components in a climate model undergoing global warming, from where water is evaporated at the surface to where it falls out as rain or snow. We determine how the relative importance of global versus local evaporation to Arctic rain and snowfall changes during global warming. As sea ice declines in response to warming, snow is eventually replaced by rain over the Arctic, the local evaporative source of snow and rain increases in all seasons, except summer. In summer, rain over the Arctic Ocean mostly comes from evaporation from land sources. In the other seasons, despite the increase of local sources of rain and snow with sea ice decline, transport of water from outside the Arctic still drives most of the Arctic rain and snowfall. Typically each individual snow or rain event is a mixture of sources indicating that local and transported water vapor are combined before raining out.

1. Introduction

Over the course of the twentieth century, the Arctic experienced an increase in precipitation (Bintanja & Andry, 2017; McCrystall et al., 2021), especially in the cold season, which has largely been attributed to anthropogenic influences (Choi et al., 2023). Most of the Arctic water vapor comes from remote sources (Peixoto & Oort, 1992), and the distribution of sources can impact the salinity of the associated marine basins (Singh et al., 2016). The variability in the poleward water vapor transport and subsequent marine export could influence salinity anomalies in the North Atlantic, and potentially the North Atlantic Oscillation (Sundby & Drinkwater, 2007) with wider impacts on the global climate system through teleconnections (e.g., Ding et al., 2023).

According to almost all climate models, Arctic precipitation will continue to increase and possibly even accelerate in the twenty-first century (McCrystall et al., 2021) with peak increases exceeding 50% over the Arctic Ocean (Cai et al., 2024). It is expected that increased local evaporation caused by sea ice retreat will contribute to fueling future precipitation trends (Bintanja & Selten, 2014). In addition, water vapor will increase, associated with retreating sea ice (Ridley et al., 2023) and water vapor transport into the Arctic may also increase with warming (Bengtsson et al., 2011) driving higher precipitation. To understand future projections of Arctic precipitation, it is important to investigate which are the dominant drivers behind the change.

There are indications from observations and reanalyses, that summer Arctic precipitation is increasingly comprised of rain (Screen & Simmonds, 2012) and it is projected that higher temperatures result in a higher percentage of Arctic precipitation falling as rain (particularly in autumn and spring) rather than snow, perhaps half of all precipitation by 2100 (Bintanja & Andry, 2017). Therefore, it is also valuable to look at the sources of Arctic rain and snow separately.

One method that can be used to trace the origin of evaporation which ends as Arctic precipitation is to use Lagrangian back tracking of water parcels in a dispersion model as done by Vázquez et al. (2016). Through forcing the model with an atmospheric reanalysis, they found that summer precipitation originates from the northern continents and winter precipitation from the subtropical oceanic regions. They also found little variation in evaporation from these regions, and consequently, variability in Arctic precipitation is related to atmospheric circulation changes. The drivers of precipitation change can also be determined using an epoch approach (piControl vs. 2100) using a combination of Atmosphere only and coupled simulations to isolate the remote and local contributions to Arctic precipitation (Leister et al., 2025).

Another method to understand changes in Arctic precipitation, associated with global warming, is through the inclusion of numerical water tracers in climate models. This was well illustrated by Singh et al. (2017) in CESM1 in which the headline result was an estimate of transported and locally sourced Arctic precipitation at double preindustrial levels of CO_2. They showed that summer precipitation is primarily driven by transport of water vapor from lower latitudes, but that winter precipitation is driven by local evaporation. An advance over the equilibrium climate study of CESM1 is to determine how the sources of Arctic precipitation change with progressive sea ice decline to the point where there is no remaining Arctic sea ice. In particular, relevant questions are:

1. Does the source of Arctic precipitation change as the sea ice declines?
2. With no more sea ice to lose, does the Arctic precipitation continue to increase, with further warming?
3. How will the precipitation changes be split between snow and rainfall and are the sources of each different?

In this study, we address these questions using water tracers in the coupled climate model HadGEM3-GC5-LL using an idealized transient simulation with carbon dioxide increasing from preindustrial levels to four times preindustrial levels. This approach not only tests the Arctic changes determined by Singh et al. (2017) using water tracers in a different climate model, but also, by using a transient climate simulation, allows us to determine whether the sources of Arctic precipitation change with extremes of future warming. We also present how the sources of rainfall and snowfall change separately in response to the warming climate.

2. Methods

Simulations using the global coupled climate model HadGEM3-GC5-LL (Xavier et al., 2026), which is the basis for the scientific configuration for CMIP7, were undertaken with the inclusion of water tracers. HadGEM3-GC5 uses the atmospheric Met Office Unified Model (UM, Willett et al., 2026) together with the JULES land surface model (Best et al., 2011; Clark et al., 2011). The atmosphere/land models are coupled to the NEMO ocean (Madec et al., 2019) and the NEMO sea ice model (SI^3, Vancoppenolle et al., 2023; Blockley et al., 2024). The version of the model used here is comprised of the Global Atmosphere and Land configuration version 9, GAL9 (Willett et al., 2026) on a regular latitude-longitude grid with a mid-latitude resolution of 135 km and 85 vertical levels. This is combined with the Global Ocean and Sea Ice configuration version 9, GOSI9 (Blockley et al., 2024; Guiavarch et al., 2025), run on a tripolar grid with a nominal resolution of 1° horizontally and 75 vertical levels.

Within GAL9, large scale precipitation (or microphysics) is modeled using a single moment scheme based on Wilson and Ballard (1999) with many modifications. The cloud parameterization scheme is the prognostic cloud fraction and prognostic condensate (PC2) scheme (Wilson et al., 2008a, 2008b). Sub-grid scale precipitation is handled by a mass flux convection scheme based on Gregory and Rowntree (1990) with several additions such as the inclusion of down-drafts (Gregory & Allen, 1991). The reader is referred to Willett et al. (2026) for further details of the atmospheric model component.

Table 1
Arctic Precipitation (in mSv) for Each Season for piControl, 2 × CO_2 and 4 × CO_2 (20-Year Mean) Periods

	Total precipitation				Snowfall				Rainfall			
Time period	DJF	MAM	JJA	SON	DJF	MAM	JJA	SON	DJF	MAM	JJA	SON
piControl	92 (19%)	93 (16%)	165 (12%)	143 (16%)	87 (20%)	85 (17%)	73 (18%)	105 (19%)	5 (6%)	8 (7%)	92 (8%)	38 (8%)
2 × CO_2	161 (37%)	130 (26%)	194 (10%)	233 (27%)	130 (42%)	96 (30%)	28 (17%)	100 (42%)	31 (16%)	34 (14%)	166 (8%)	133 (16%)
4 × CO_2	281 (44%)	212 (31%)	226 (9%)	343 (24%)	115 (59%)	80 (46%)	0	14 (57%)	166 (33%)	132 (23%)	226 (9%)	329 (23%)

Note. The percentage of each precipitation type that is locally sourced (from both open ocean evaporation and sea ice sublimation) is shown in brackets.

A preindustrial control (piControl) is initialized, after 800 years of spin-up, using CMIP6 forcings (Eyring et al., 2016). Climate change is simulated through an idealized 1% increase in carbon dioxide per year (1pctCO2). The 1pctCO2, simulation (Eyring et al., 2016) is initialized from the piControl and is 150 years in length reaching 2 × CO_2 at year 70 and 4 × CO_2 at year 140. The HadGEM3-GC5 1pctCO2 experiment has no interactive vegetation or carbon cycle, it maintains aerosols and land use characteristics at the preindustrial state from the CMIP6 forcings data set (Eyring et al., 2016). At the end of the 1pctCO2 simulation, at 4 times preindustrial CO_2, the Arctic in HadGEM3-GC5-LL is completely ice-free in all seasons. 20-year mean time slices are presented in the paper, centered on year 70 for 2 × CO_2 and on year 140 for 4 × CO_2. These are compared with a piControl 20-year mean.

McLaren et al. (2025) added numerical water tracers to the UM that follow water throughout the model. This involved adding water tracers to the following schemes: surface evaporation, large-scale advection, boundary layer mixing, large-scale precipitation, large-scale clouds, stochastic physics and convection. The water tracers were found to track all the water in the model to a high degree of accuracy.

The water tracers used in this paper follow the "prescribed-region" tracer method described by McLaren et al. (2025). As the model simulation progresses, the Eulerian water tracers track the evaporated water from various prescribed surface regions through the atmosphere model until it reaches the surface as precipitation or surface condensation. To determine the sources of Arctic precipitation, the tracers separately track the evaporation from open ocean, the sublimation from sea ice and evapotranspiration from land. The tracers are then further split into relevant geographic regions creating 14 prescribed regions which cover the global domain (Table A1). The water tracers thus provide the amount of precipitation at each model grid box that has been sourced from each prescribed region.

We define the Arctic as the *ocean* domain north of 60°N in the Pacific sector and north of 70°N in the Atlantic sector (as shown by the pink region in Figure 1). This excludes some of the initially sea ice covered regions as indicated by the sea ice edge contour in Figure 1. The Arctic area definition covers four of the open-ocean water tracer prescribed regions (tracers numbered 7, 9–11 in Table A1) and these four tracers are aggregated in the analysis to provide the open-ocean Arctic sourced contribution. This is combined with the tracer tracking

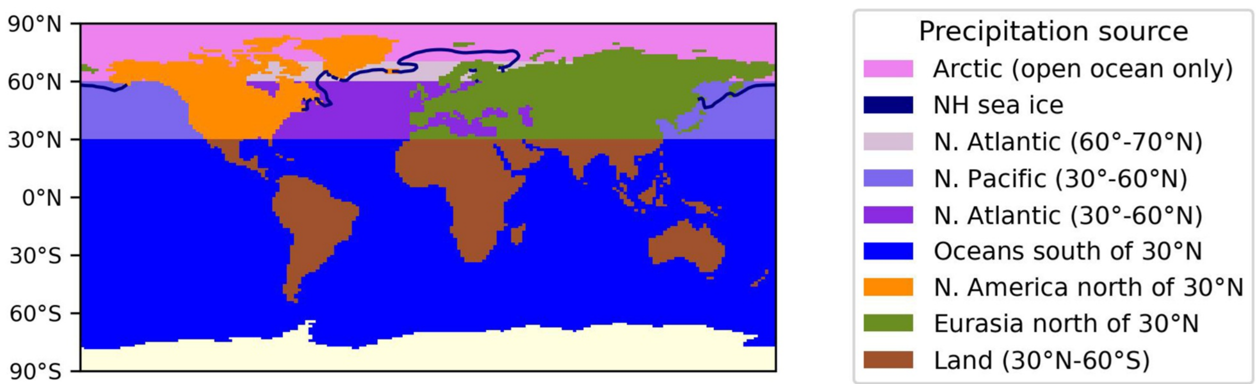

Figure 1. The simplified prescribed water tracer regions considered in this paper. The Arctic is defined as all the ocean in the pink region. The solid navy-blue line is the 15% annual mean sea ice concentration contour at the start of the 1pctCO2 simulation and indicates the water tracer that tracks sublimation from NH sea ice.

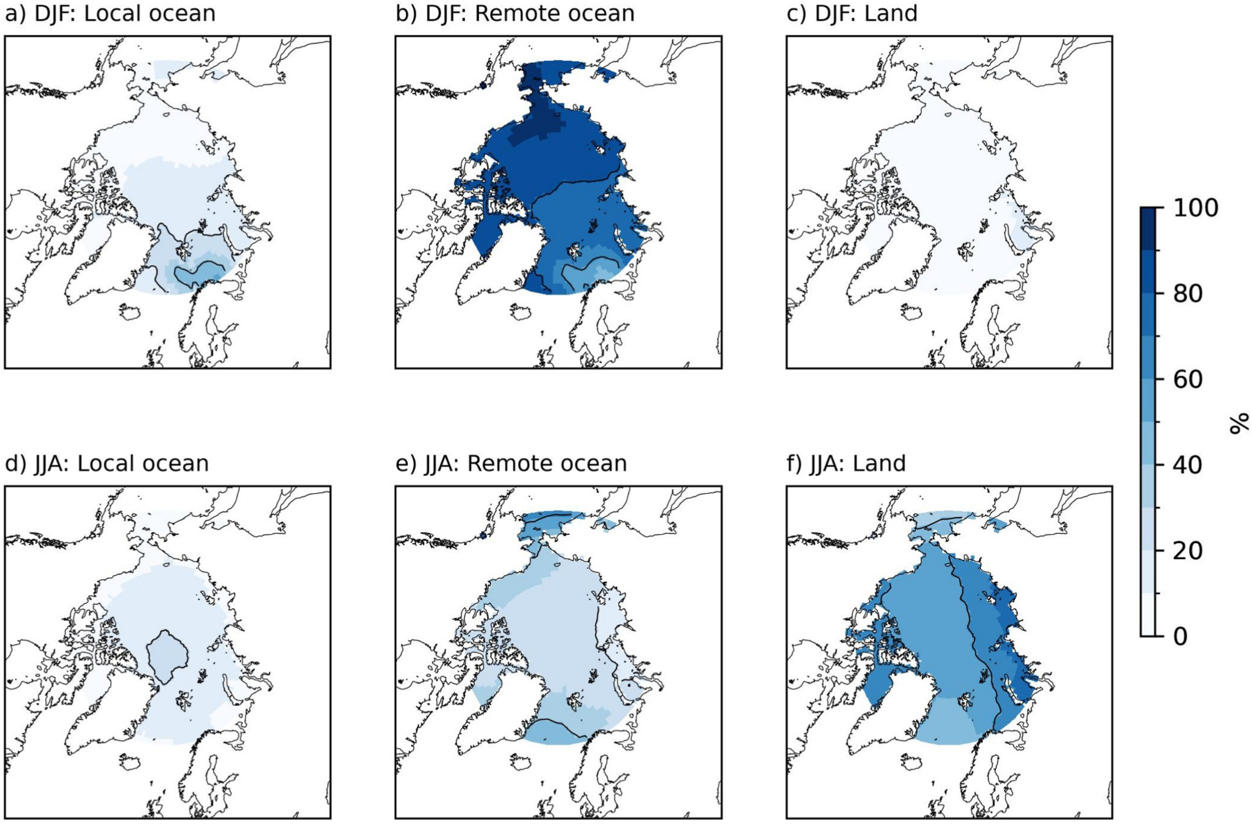

Figure 2. Percentage of Arctic precipitation from 20 years of the piControl experiment for DJF (top row) and JJA (bottom row) sourced from: (a, d) local ocean evaporation and sea ice sublimation; (b, e) remote ocean evaporation; and (c, f) remote land evapotranspiration. Black contour lines are shown for 20%, 40%, 60% and 80%.

sublimation from the NH sea ice (tracer number 2) to give the total "local" contribution to Arctic precipitation. The remaining water tracers track "remote" sources of Arctic precipitation from the regions shown in Figure 1. The inclusion of the NH sea ice tracer in the local contribution will cause a slight overestimate of this term as this includes sublimation from sea ice outside of the defined Arctic region. However, as shown in McLaren et al. (2025), the precipitation sourced from Arctic sea ice sublimation is focused in the Central Arctic, so this overestimation will remain small.

3. Results

3.1. Preindustrial Climate

The base state of the climate model is defined through the preindustrial simulation, the start point of the 1pctCO2 simulation. Within this state we examine the Arctic total precipitation (Figure 2), in winter (December January and February, DJF) and summer (June July and August, JJA), dividing it broadly into source regions of local ocean, remote ocean and land.

In winter the high latitude land is snow-covered, and the local ocean is sea ice covered. Consequently, most precipitation falling in the Arctic in winter is sourced (evaporated) from remote ocean locations (Figure 2b). Transport into the Arctic during winter typically occurs in episodic, high-amplitude events with strong impacts on the Arctic's climate system components including sea ice (Papritz et al., 2022). Many of these events are cyclones originating from the Atlantic and Pacific storm tracks. Fearon et al. (2021) suggests that these are responsible for 74% of poleward water vapor transport. The component sourced from the local ocean (Figure 2a) evaporates from the open water part of the Barents Sea and from leads in the sea ice. The component sourced from land (Figure 2c) must be transported from southwards of the snowline, with a small component as snow sublimation.

In summer, vegetation across the snow-free land undergoes evapo-transpiration, resulting in it being a dominant contributor to remotely sourced precipitation (Figure 2f). It is thought that the transport mechanism from land and remote ocean is through low frequency circulation changes (blocking) and atmospheric rivers (Wang et al., 2024). In summer the local ocean sourced evaporation (Figure 2d) is low with a small component from sea ice sublimation.

3.2. The Transient Simulation

Here we present the changes in precipitation sources during the 1pctCO2 simulation through stacked Hovmoller plots, displaying the absolute Arctic precipitation in milli Sverdrups (1 mSv = 10^3 m^3 s^{-1}) by source region. We also show the relative contribution of the sources to the total precipitation as a means to determine how the sources are changing in time.

The same seasonal pattern as observed in Figure 2 is seen in year zero (preindustrial) in Figure 3. Summer has the greatest precipitation, with approximately 60% of precipitation sourced from Eurasia and North American land masses and a few percent sublimated from sea ice. In winter, approximately 15% comes from the tropical ocean, 20% from the North Atlantic, and 20% from the North Pacific. If the main transport mechanism to the Arctic is cyclones (Fearon et al., 2021), then these results show that some of the water vapor in cyclones from the tropics (i.e., oceans south of 30°N) remains in the system as far north as the Arctic. The autumn and spring precipitation sources are transitions between summer and winter sources.

The precipitation increases in each season with the enhancement of the hydrological cycle during the transient simulation. The largest increase by 4 × CO_2 (year 140) is in winter with a tripling of precipitation; the smallest change is in summer with a 37% increase. These changes should be compared with a global annual mean change of 14% over the same period. The Arctic changes are larger than global trends due to the import of water, local evaporation following the decline of sea ice cover with warming and polar amplification. In winter, the amount of precipitation of local origin increases from 19% to 44%, with similar, but lower fractional increases in spring and autumn. The winter increase in local evaporation is aided though an increase in windspeeds that is greater than in other seasons; the mean Arctic 10 m wind speed increases at a rate of 0.118 ms^{-1} per decade for winter, compared to 0.075 ms^{-1} per decade for autumn. The increase in winter wind speed has been linked to the destabilization of the atmosphere (Zapponini & Goessling, 2024). As sea ice declines, the fraction of locally sourced precipitation increases, but once all seasonal sea ice is lost, there is no more change in its relative fraction. However, in the absolute sense, the precipitation continues to increase due to the increased atmospheric capacity to hold water vapor (Clausius-Clapyron) with continued warming (Ridley et al., 2023).

The smallest change in precipitation occurs in summer (Figure 3c) when evaporation on the continents is the dominant source. Arctic sourced precipitation is low due to weak winds and a small difference between atmosphere and ocean surface temperature, which does not change with warming (Ridley et al., 2016). The small component sourced from sea ice sublimation is replaced by open ocean evaporation sources as the sea ice declines. In the latter half of the simulation, the percentage of precipitation sourced from the ocean increases slightly so that the ocean and land sourced precipitation amounts are very similar by year 150.

Arctic sea ice persists for the shortest time in autumn (Figure 3d), and there is a strong precipitation source from the North Atlantic and Pacific, likely propagated due to storms (Ridley et al., 2023). The spring ice cover (Figure 3b) survives longer than in autumn, but the sources of precipitation in the two seasons are similar. Interannual variability causes a slight recovery in the summer and autumn sea ice area around year 60, associated with a decrease in Arctic surface temperatures. Subsequently, the locally sourced precipitation in the autumn temporarily ceases to increase over this period (Figure 3d). The initial state has summer with the highest precipitation, but the increased rate of change of precipitation with warming, due to sea ice decline, in the other seasons results in the highest precipitation at 4 × CO_2 being in autumn and winter.

Total precipitation can be broken down into snowfall (Figure 4) and rainfall (Figure 5) to determine if the types of precipitation are differently sourced. At the start of the simulation, snow dominates over rainfall in all seasons, apart from summer, where approximately 60% of precipitation falls as rain. In general, the snowfall increases to the point where sea ice has near disappeared and then diminishes as the local air temperatures, over a warmer ocean, are too high to sustain it. By 4 × CO_2, most Arctic snow is locally sourced. The situation in summer (Figure 4c) is slightly different as the snowfall declines from early in the simulation along with sea ice cover.

10.1029/2026JD046751

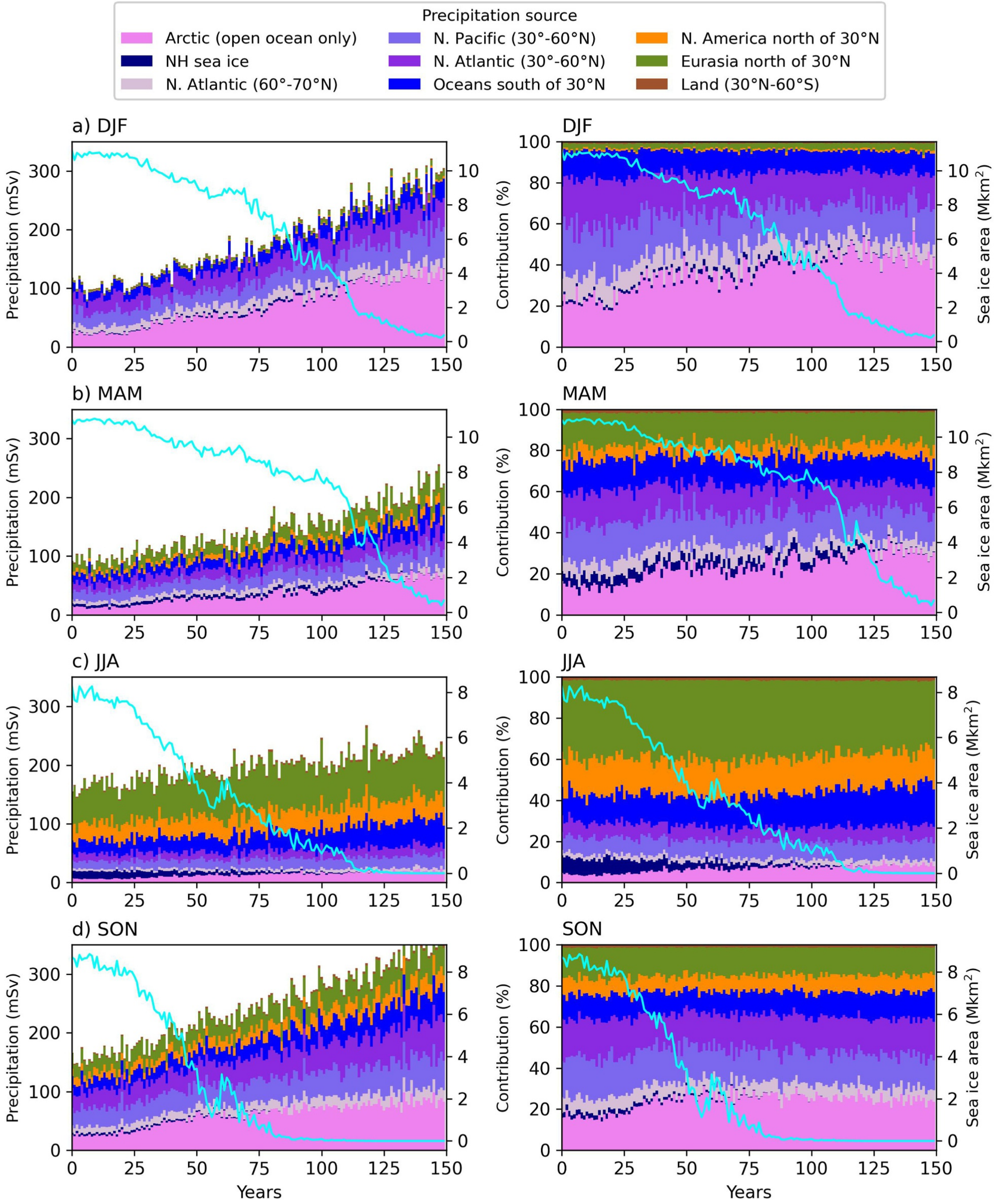

Figure 3. The modeled evolution of the sources of Arctic total precipitation through the 1pctCO2 simulation for each season. The column on the left shows the absolute values (mSv) and the column on the right for the relative contributions (%) from the different source regions. The cyan solid line is the total sea ice area (Mkm^2) in the region defined as the Arctic, with the axis shown on the right of the plots. (Note, 100 mSv is approximately 3×10^3 km^3 yr^{-1}).

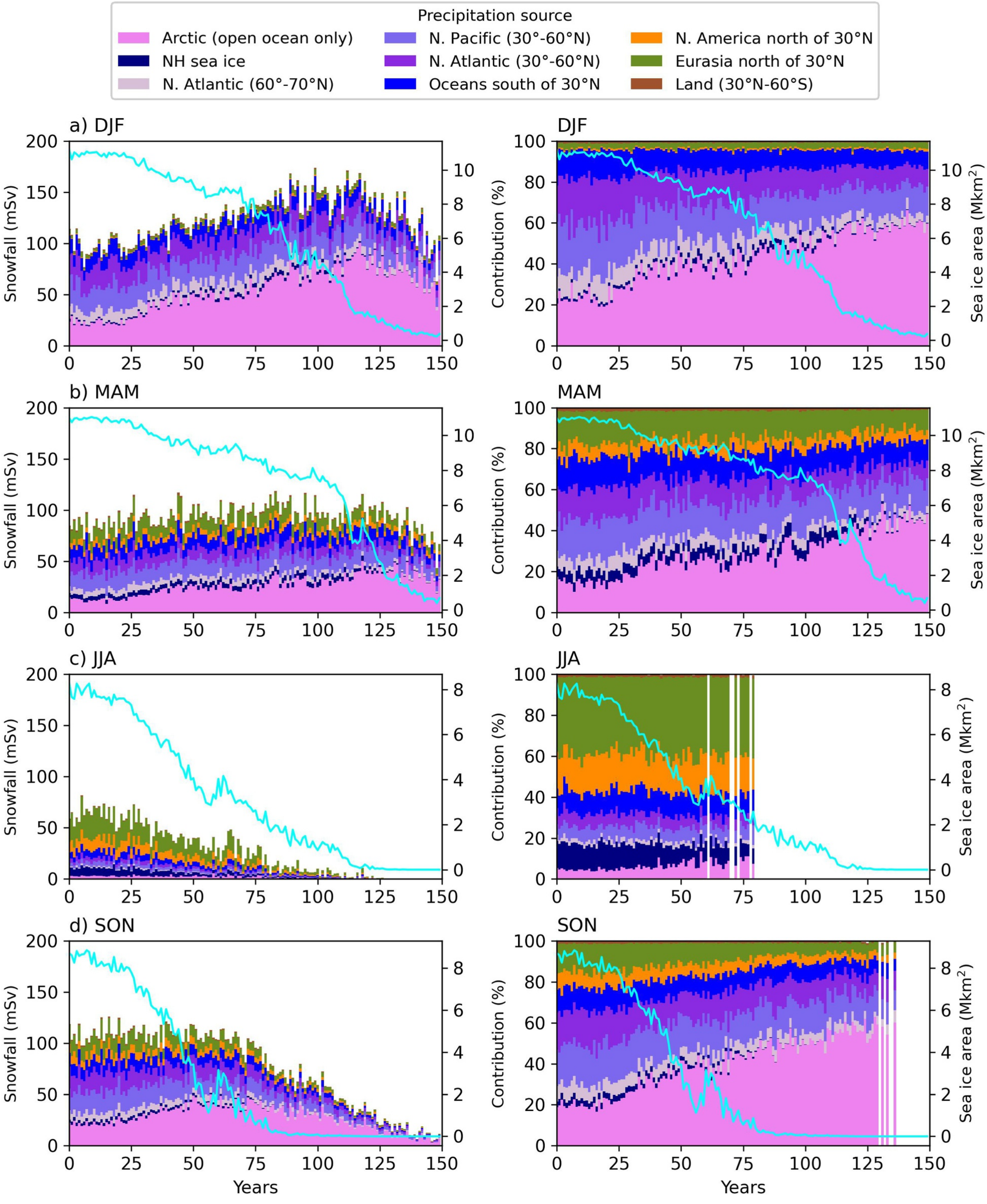

Figure 4. As Figure 3 but for snowfall only. (The relative contribution is only plotted when Arctic snowfall is greater than 20 mSv.)

The point in the timeseries where snowfall starts to diminish, and rainfall increase (Figures 4 and 5) is linked to the rapid decline in sea ice area. Rainfall amounts become consistently larger than snowfall around the model years 130, 120 and 50 for DJF, MAM and SON respectively. Even in winter (Figure 5a) there is locally sourced Arctic rainfall, following the loss of sea ice, resulting in a warmer ocean and air temperature. However, the proportion of

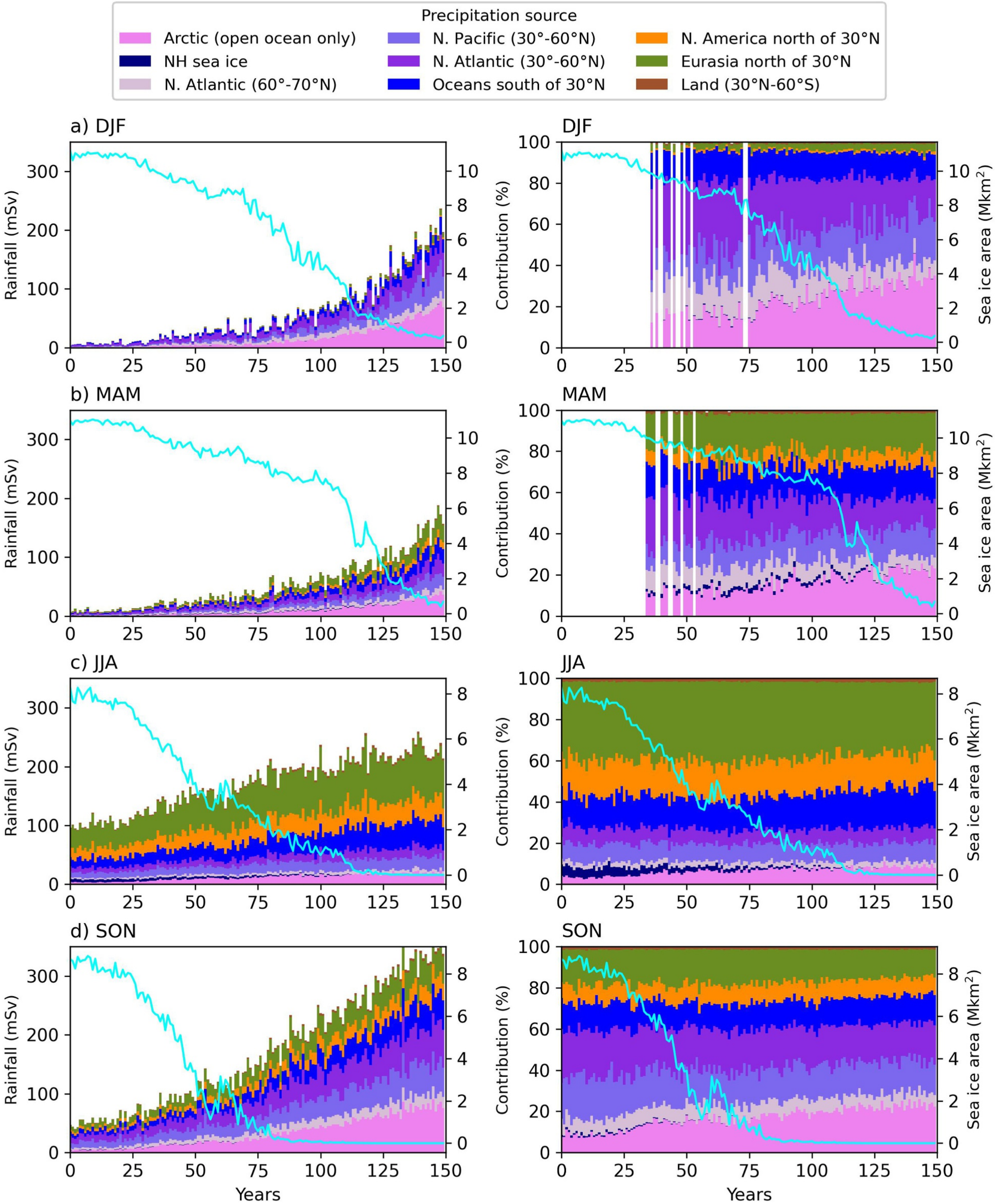

Figure 5. As in Figure 3, but for rainfall only. (The relative contribution is only plotted when Arctic rainfall is greater than 20 mSv).

rainfall sourced from the Arctic is less than that for snowfall. Since the southern bounds of the Arctic are the warmest, rain predominately falls at the fringes of the Arctic and will therefore be more likely to have sources classed as remote. This also highlights that the proportion of rain to snow may be influenced by the size of the

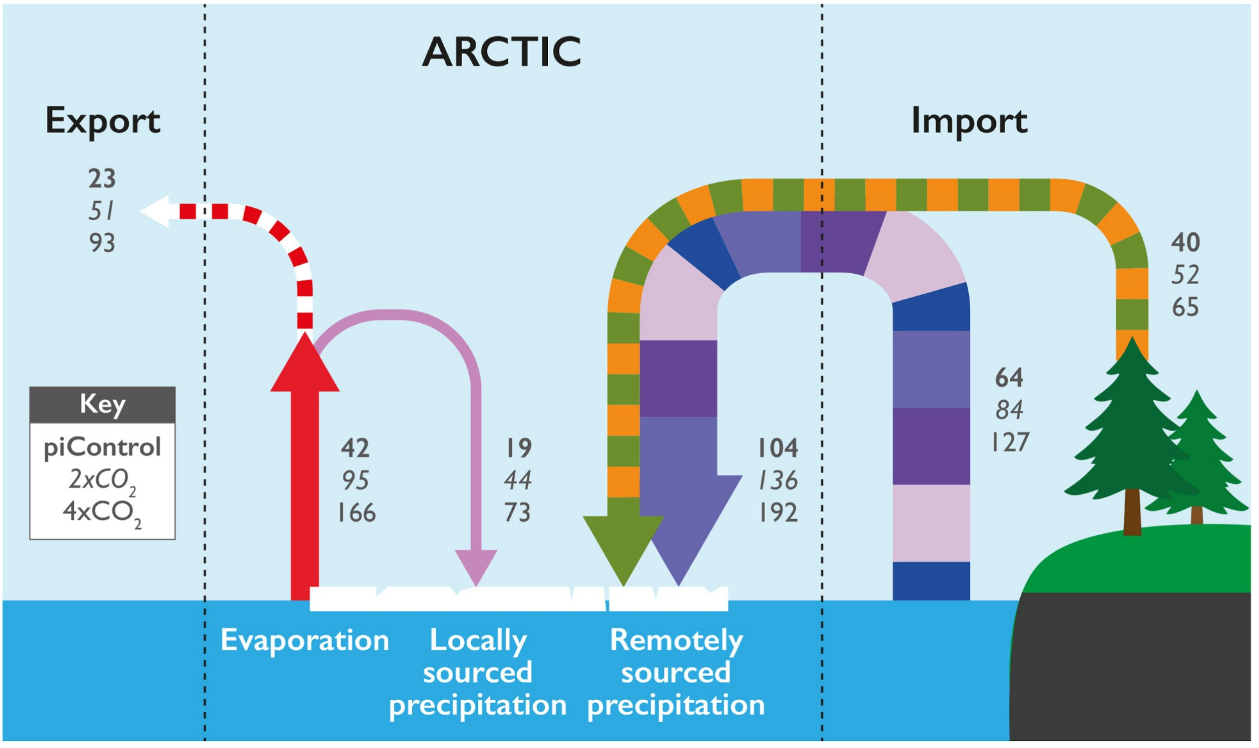

Figure 6. Annual mean water budget for the Arctic (mSv) for piControl, $2 \times CO_2$ and $4 \times CO_2$ (20-year means) with illustrative arrows showing sources with colors that match Figures 2–5. The locally and remotely sourced precipitation amounts are derived from the water tracer information. Evaporation is the net sea evaporation plus sea ice sublimation. The export from the Arctic is calculated by subtracting the locally sourced precipitation amount from the Arctic net evaporation/sublimation.

domain. In summer (Figure 5d), rainfall is always the dominant phase of precipitation. The combination of snow and rain results in a linear increase in total precipitation with warming as found globally.

A summary of Figures 3–5 is provided at key temporal intervals in Table 1. Total precipitation and rainfall increase, with CO_2, and temperature, in all seasons. In all seasons, the total precipitation is dominated by remote sources. Snowfall first increases then declines in winter and spring and declines from the start of summer and autumn. The fraction of snowfall and rainfall that is locally sourced increases substantially with increasing CO_2 (and sea ice decline), in all seasons except summer; the increase in the locally sourced fraction of rainfall is less than for snowfall.

The model's Arctic annual mean water budget for the 20-year mean periods for piControl, $2 \times CO_2$ and $4 \times CO_2$ is presented in Figure 6. This highlights that on the annual scale remotely sourced precipitation dominates in the Arctic during all the time periods. At $2 \times CO_2$, the increase in Arctic precipitation is driven by an additional 32 mSv from remote sources and 25 mSv from local sources. By $4 \times CO_2$, the precipitation increase is mostly driven by remote sources (62%). More than half of the evaporation from the Arctic ocean is exported (Figure 6) (i.e., it does not fall as local precipitation) and this changes little in the 1pctCO2 experiment with 54% exported in the piControl compared with 56% at $4 \times CO_2$.

3.3. Daily Precipitation Sources

So far, we have discussed seasonal mean diagnostics from HadGEM3-GC5-LL which show a mix of local and remote sources. We look now at daily diagnostics to determine if the individual precipitating days in the Arctic are from a single source or mixed sources. To illustrate this, we look at a timeseries of a representative single grid cell in the central Arctic for the winter season at $4 \times CO_2$, when local sources dominate remote sources on the seasonal scale, and no sea ice remains in the Arctic.

The daily timeseries (Figure 7) shows days with a mix of local and remote sources. On some days the local source dominates and on other days a combination of local and remote sources is present. This suggests that, depending

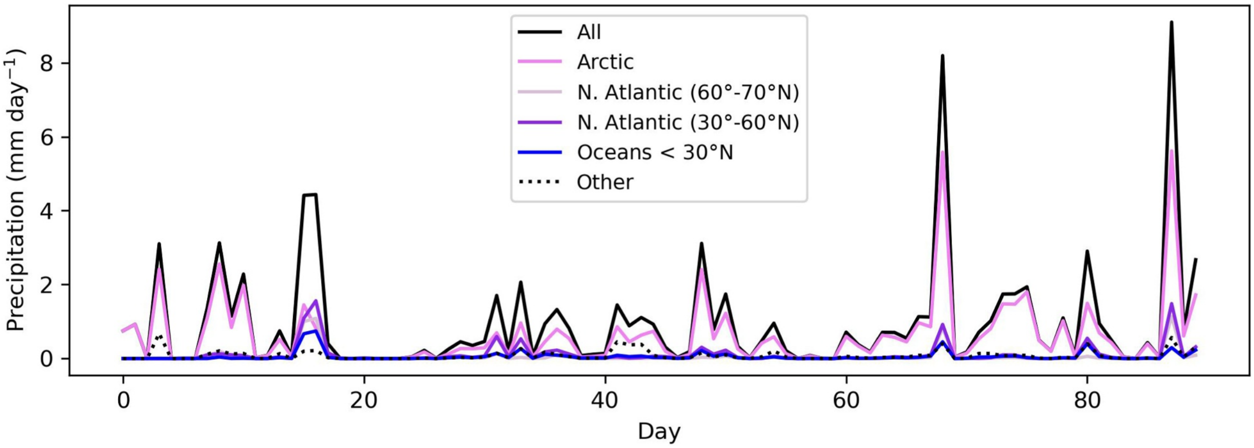

Figure 7. Example 90-day timeseries in DJF during 4 × CO2 period at a point in the Central Arctic (84.5°N, 14.1°E) showing daily precipitation and the individual sources (in mm day^{-1}). The location of this example point is shown by the red cross in Figure 8.

on the daily meteorology, the mixing of remote and local sources can occur. This is not surprising as water vapor remains in the atmosphere for 8–10 days (Gimeno et al., 2021), long enough for air masses from various sources to mix prior to precipitation. Indeed, warming is projected to increase residence time, lengthening the distance traveled between evaporation sources and precipitation sinks (Gimeno et al., 2021), so potentially greater mixing from various sources.

In order to assess the amount of mixing over the whole Arctic and contextualize the example grid point in Figure 7, the daily precipitation at each model grid point in the Arctic is binned according to the locally sourced fraction. This is done for 20 years of winter data at $4 \times CO_2$ (Figure 8). As an illustration to aid interpretation of Figure 8, the results at the example point (shown by the red cross) indicate that 60% of the precipitation over the 20-year winter period falls on days when the locally sourced fraction is between 0.25 and 0.75. Only 22% of total precipitation falls on days when the locally sourced fraction is greater than 0.75. The remaining 18% of total precipitation then occurs on days when the locally sourced fraction is less than 0.25.

The spatial pattern of total precipitation is presented in Figure 8a showing that even in the absence of sea ice, the strongest precipitation is at the fringes of our Arctic domain. The areas dominated by remote precipitation on the daily scale (<0.25 local fraction) produce a high percentage of the marginal pattern (Figure 8b) with very little penetrating to the central Arctic. Such a pattern is consistent with water-rich cyclones dying out as they reach the colder waters and precipitating out. This suggests that the size of the Arctic domain may influence the fraction of remotely sourced precipitation. The intermediate mixing of sources (Figure 8c) shows an opposite pattern with a large percentage of the low precipitation regions in the central Arctic being of mixed sources. With a pattern including the high precipitation region of the Norwegian Sea it is suggestive of Atlantic water penetration deep into the Arctic mixing with locally sourced evaporation. When locally sourced precipitation dominates (Figure 8d), it is widely spread across the central Arctic. Overall, this shows that in the Central Arctic, there is a mix of local and remote sources both on the daily and seasonal timescales.

4. Conclusions

The incorporation of water tracers in HadGEM3-GC5 has enabled an assessment of the evaporation sources of seasonal and daily precipitation in the Arctic. This has shown that both local and remote sources contribute to precipitation on the daily and seasonal timescales. We have focused on the sources of Arctic precipitation using an idealized transient simulation of 1% per annum increase of CO_2 to $4 \times CO_2$ over 150 years. Summer displays the smallest increase in total precipitation (37%), with autumn and winter the greatest (140% and 205% respectively). In agreement with other studies (e.g., Bintanja & Selten, 2014), these changes are much larger than the global trend; the global annual mean change being 14% over the same period. As time progresses, sea ice retreats, leading to an increase in locally sourced precipitation falling in the Arctic and a switch from snowfall to a rain-dominated Arctic. However, throughout the simulation there is no season in which the total precipitation is dominated by local sources. The external sources of precipitation change according to season with winter arriving

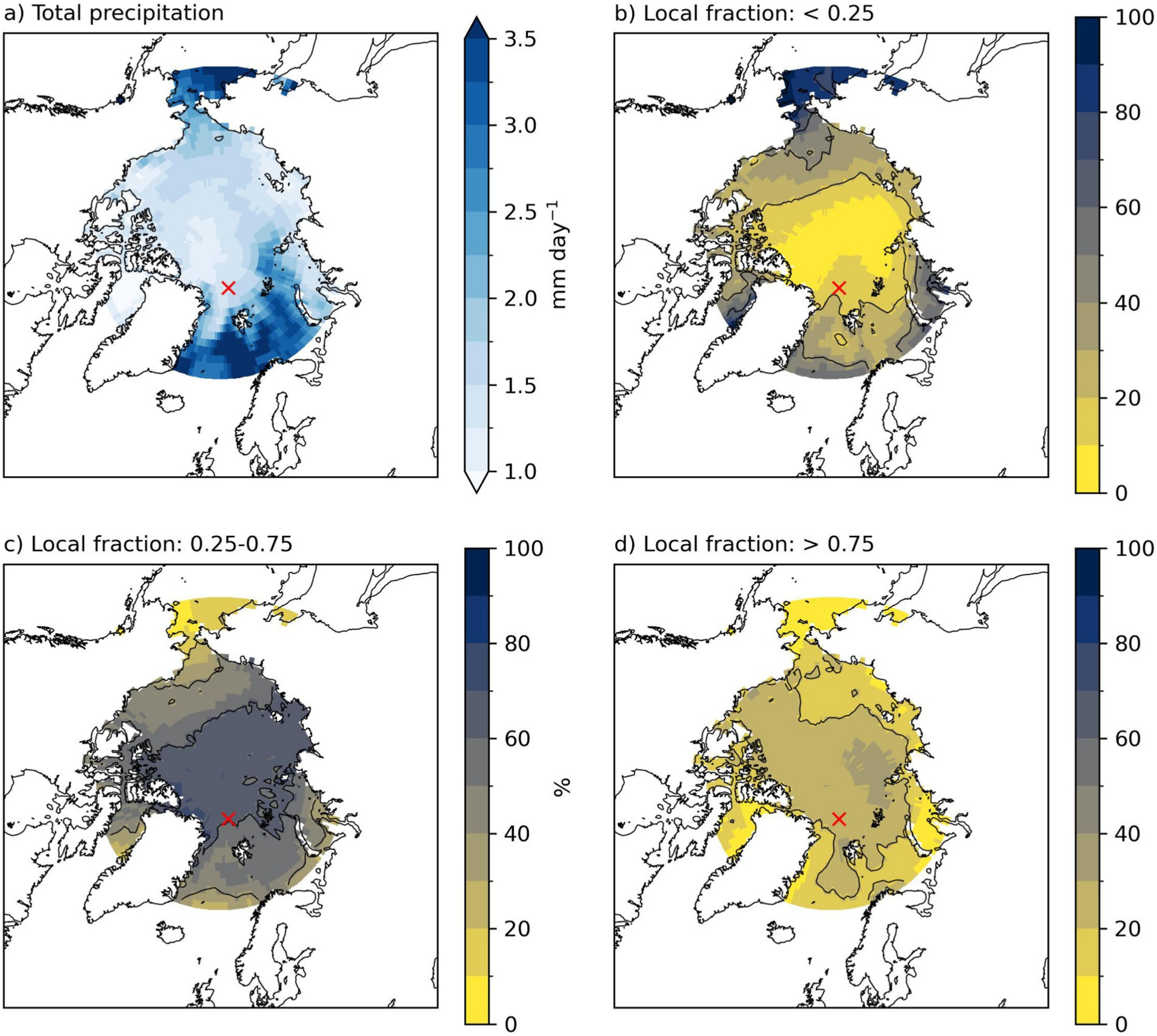

Figure 8. Arctic precipitation from 20 years of DJF centered at 4 × CO_2: (a) Total precipitation (mm day^{-1}); (b–d) Percentage of total precipitation that occurs when the daily locally sourced fraction is (b) <0.25; (c) 0.25–0.75; (d) >0.75 (Days with precipitation less than 0.1 mm day^{-1} are omitted from this analysis). The red cross indicates the location of the example timeseries shown in Figure 7.

primarily from ocean sources (North Atlantic, North Pacific and Tropics), whilst summer precipitation is mainly sourced from the land (Eurasia and North America). Spring and autumn are intermediate in precipitation sources to summer and winter. Rain is more likely to be externally sourced than snowfall, but the remote sources of rainfall and snowfall show no significant differences.

In terms of the annual mean water budget of the Arctic, the locally sourced precipitation increases from 15% in the preindustrial experiment to 38% at 4 × CO_2. The increase in Arctic precipitation at 4 × CO_2 of 142 mSv is found to come primarily from remote oceans (63 mSv) and local sources (54 mSv), with the remaining increase coming from land sources. The annual budget reveals that approximately 55% of Arctic evaporation is exported from the region and this percentage changes little with increasing CO_2. This highlights the importance of using techniques like numerical water tracers to carefully track evaporation sources since it is otherwise hard to detect or track the influence of Arctic export of water vapor.

An original analysis of daily winter precipitation events when the Arctic is ice-free reveals that on average each event is comprised of a mix of air masses from different remote locations and local sources. This is during a period when 44% of precipitation is locally sourced on the seasonal scale. There is significant spatial variability with remote air masses dominating precipitation sources at the Arctic margins whilst locally sourced precipitation becomes increasingly important in the central Arctic. Given that the mean atmospheric residence time of water vapor is 8–10 days (Gimeno et al., 2021), it is unsurprising that the daily analysis indicates that water vapor from many sources is mixed enroute to and within the Arctic during a substantial number of Arctic precipitation events.

The above findings, those of the summer continental and winter marine sources of precipitation, are in general agreement with previous studies from climate models. Singh et al. (2017) used water tracers but in the CESM climate model to investigate the difference between preindustrial CO_2 and an equilibrium $2 \times CO_2$ experiment. Both Singh et al. and this study show similar relative changes in precipitation by season, and that the increase in Arctic precipitation is mainly driven by the remote contribution. This indicates that both models agree on the general properties of transport of poleward water vapor transport, despite having different model details of the hydrological cycle. However, it should be noted that CESM has considerably more Arctic precipitation than HadGEM3, even when the same Arctic definition is used; Singh et al. (2017) define the "Arctic" as a larger region (>60°N) than the one used here. This is not surprising as Bintanja and Selten (2014) showed that the amount of Arctic annual mean precipitation varied by a factor of 3 across CMIP5 models. A limitation of this study is the inability to verify the numerical water tracers directly against observations. In future, the comparison of water isotopes in the model against equivalent satellite and in situ observations could provide a means to indirectly evaluate water tracer properties (Bong et al., 2024; Gao et al., 2025; Nusbaumer et al., 2017; Tindall et al., 2009).

The increase in local precipitation, because of sea ice decline, was discussed by Bintanja and Selten (2014), with the magnitude of the seasonally locally sourced component greater than ours. However, their budget method did not account for the export of local evaporation, which we have shown to be very significant (55%) in the Arctic hydrological cycle. We find a transition from a snow-dominated to rain-dominated Arctic, previously noted by Bintanja and Andry (2017), and like Tsakali et al. (2025) we find that a new rain-dominated climate state arises in response to sea ice decline.

This study uses idealized transient CO_2 forcing in order to obtain a clear signal of the impact of increasing global temperature on the Arctic hydrological cycle. HadGEM3-GC5-LL has a very high effective climate sensitivity of 6.7 K as discussed in Rostron et al. (2026). Therefore, the magnitude of the global warming signal is expected to be particularly strong in this idealized study. The impact of the model's climate sensitivity on the results could be investigated further by repeating the water tracer experiments with a new configuration of HadGEM3-GC5-LL, named UKCM2-LL, which has a much lower effective climate sensitivity of 3.6 K (Rostron et al., 2026).

The model experiments use the low resolution version of HadGEM3 with an atmosphere resolution of 135 km at mid-latitudes and a 1° ocean resolution. The sensitivity of the Arctic hydrological cycle to resolution has previously been investigated by Ridley and Blockley (2025) in the CMIP6 version of HadGEM3. They found that the total precipitation and hydrological stores over Arctic land were insensitive to model resolution when comparing low resolution to mid resolution (60 km in the atmosphere, ¼° in the ocean) simulations. The only exception was faster declining snowfall rates and snow volumes over land at low resolutions, due to smoother orography impacting orographically induced precipitation. This suggests that our water tracer analysis of the hydrological cycle over the Arctic Ocean would be robust across low and mid resolutions. Further work would be required to investigate the response at higher resolutions.

Given that evapotranspiration from land sources drives most of the summertime Arctic precipitation, a potential limitation of this present study is the lack of an interactive vegetation model that would respond to global warming and land use changes (Clark et al., 2011). This could be investigated by running the same numerical water tracers in the UK Earth System Model (Sellar et al., 2019). It is also noted that the exact findings of this analysis will be sensitive to the definition of the Arctic, especially as most precipitation falls at the Pacific and Atlantic margins of the Arctic domain, about three times that in the central Arctic.

Observations indicate that precipitation in the Arctic is increasing. Climate models predict that Arctic precipitation will continue to increase and accelerate in the twenty-first century. We have shown that numerical water tracers can indicate which source regions drive this increase. The principal change is an increase in locally sourced evaporation as sea ice retreats. Once there is no remaining Arctic sea ice sources do not change further, despite continued warming. This study, combined with those of other models, provides a compelling case that numerical water tracers provide a robust analysis of regional hydrological cycles within climate models.

Appendix A

For the purposes of the model analysis presented in the paper, this list is reduced and amalgamated. It is found that precipitation in the Arctic sourced from southern sea ice (water tracer number 3) and Antarctica (number 12) do not contribute significantly to the precipitation in the Arctic, consequently they are removed from further consideration. The ocean regions in the high latitude Arctic (water tracer numbers 7, 9, 10 and 11) are combined to match the definition of the Arctic used in this paper. The first water tracer tracks all the water in the model and is used to monitor the accuracy of the water tracer scheme. Table A1.

Table A1
The Water Tracer Prescribed Regions From Which Evaporation is Tracked in the Model Experiments

Water tracer number	Prescribed regions
1	Full globe (normal water tracer)
2	NH sea ice
3	SH sea ice
4	Open ocean south of 30°N
5	Open ocean 30–60°N, 101–262°E (N. Pacific)
6	Open ocean 30–60°N, 262°E > 0 > 101°E (N. Atlantic/Mediterranean)
7	Open ocean 60–70°N, 101–262°E (Bering and Chukchi seas)
8	Open ocean 60–70°N, 262°E > 0 > 101°E (Sub-polar Atlantic)
9	Open ocean 70–80°N, 101–262°E (Arctic—Pacific sector)
10	Open ocean 70–80°N, 262°E > 0 > 101°E (Arctic—Atlantic sector)
11	Open ocean north of 80°N (Central Arctic)
12	Land south of 60°S
13	Land between 30°N and 60°S
14	Land north of 30°N and 191°E–348°E (North America/Greenland)
15	Land north of 30°N and between 348°E > 0 > 191°E (Europe/Asia)

Conflict of Interest

The authors declare no conflicts of interest relevant to this study.

Availability Statement

The processed data and python code to generate the figures in this paper may be found at https://doi.org/10.5281/zenodo.18611155 (McLaren & Ridley, 2026).

Acknowledgments
Jeff Ridley and Ed Blockley were supported by the Met Office Hadley Centre Climate Programme funded by DSIT. Alison McLaren and Louise Sime were supported by: NERC UK Polar Research Expertise for Science and Society (PRESCIENT; Grant. NE/Y006178/1), NERC Sensitivity of the West Antarctic Ice Sheet to +2°C (SWAIS2C; Grant. NE/X009386/1), and NERC Surface Fluxes in Antarctica (SURFEIT; Grant. NE/X009319/1), and Department for Business, Innovation, Science and Trade.

References

Bengtsson, L., Hodges, K. I., Koumoutsaris, S., Zahn, M., & Keenlyside, N. (2011). The changing atmospheric water cycle in polar regions in a warmer climate. *Tellus Series A-Dynamic Meteorology and Oceanography*, *63*(5), 907–920. https://doi.org/10.1111/j.1600-0870.2011.00534.x

Best, M. J., Pryor, M., Clark, D. B., Rooney, G. G., Essery, R. L. H., Ménard, C. B., et al. (2011). The joint UK land environment simulator (JULES), model description – Part 1: Energy and water fluxes. *Geoscientific Model Development*, *4*(3), 677–699. https://doi.org/10.5194/gmd-4-677-2011

Bintanja, R., & Andry, O. (2017). Towards a rain-dominated arctic. *Nature Climate Change*, *7*(4), 263–267. https://doi.org/10.1038/nclimate3240

Bintanja, R., & Selten, F. (2014). Future increases in arctic precipitation linked to local evaporation and sea-ice retreat. *Nature*, *509*(7501), 479–482. https://doi.org/10.1038/nature13259

Blockley, E., Fiedler, E., Ridley, J., Roberts, L., West, A., Copsey, D., et al. (2024). The sea ice component of GC5: Coupling SI3 to HadGEM3 using conductive fluxes. *Geoscientific Model Development*, *17*, 6799–6817. https://doi.org/10.5194/gmd-17-6799-2024

Bong, H., Cauquoin, A., Okazaki, A., Chang, E.-C., Werner, M., Wei, Z., et al. (2024). Process-based intercomparison of water isotope-enabled models and reanalysis nudging effects. *Journal of Geophysical Research: Atmospheres*, *129*(1), e2023JD038719. https://doi.org/10.1029/2023JD038719

Cai, Z., You, Q., Chen, H. W., Zhang, R., Zuo, Z., Chen, D., et al. (2024). Assessing arctic wetting: Performances of CMIP6 models and projections of precipitation changes. *Atmospheric Research*, *297*, 107124. https://doi.org/10.1016/j.atmosres.2023.107124

Choi, H. J., Min, S. K., Yeh, S. W., & Kim, B. M. (2023). Seasonally distinct contributions of greenhouse gases and anthropogenic aerosols to historical changes in arctic moisture budget. *npj Climate and Atmospheric Science*, *6*(1), 189. https://doi.org/10.1038/s41612-023-00518-9

Clark, D. B., Mercado, L. M., Sitch, S., Jones, C. D., Gedney, N., Best, M. J., et al. (2011). The joint UK land environment simulator (JULES), model description – Part 2: Carbon fluxes and vegetation dynamics. *Geoscientific Model Development*, *4*(3), 701–722. https://doi.org/10.5194/gmd-4-701-2011

Ding, R., Nnamchi, H. C., Yu, J. Y., Li, T., Sun, C., Li, J., et al. (2023). North Atlantic oscillation controls multidecadal changes in the North Tropical atlantic−pacific connection. *Nature Communications*, *14*(1), 862. https://doi.org/10.1038/s41467-023-36564-3

Eyring, V., Bony, S., Meehl, G. A., Senior, C. A., Stevens, B., Stouffer, R. J., & Taylor, K. E. (2016). Overview of the coupled model intercomparison project phase 6 (CMIP6) experimental design and organization. *Geoscientific Model Development*, *9*(5), 1937–1958. https://doi.org/10.5194/gmd-9-1937-2016

Fearon, M. G., Doyle, J. D., Ryglicki, D. R., Finocchio, P. M., & Sprenger, M. (2021). The role of cyclones in moisture transport into the arctic. *Geophysical Research Letters*, *48*(4), e2020GL090353. https://doi.org/10.1029/2020GL090353

Gao, Q., Sime, L. C., McLaren, A. J., & Werner, M. (2025). Moisture source controls on water isotopes in Antarctic precipitation—Insights from water tracers in ECHAM6-wiso. *Journal of Geophysical Research: Atmospheres*, *130*(15), e2024JD043047. https://doi.org/10.1029/2024JD043047

Gimeno, L., Eiras-Barca, J., Durán-Quesada, A. M., Dominguez, F., van der Ent, R., Sodemann, H., et al. (2021). The residence time of water vapour in the atmosphere. *Nature Reviews Earth & Environment*, *2*(8), 558–569. https://doi.org/10.1038/s43017-021-00181-9

Gregory, D., & Allen, S. (1991). The effect of convective downdraughts upon NWP and climate simulations. In *Ninth conference on numerical weather prediction* (pp. 122–123).

Gregory, D., & Rowntree, P. R. (1990). A mass flux convection scheme with representation of cloud ensemble characteristics and stability-dependent closure. *Monthly Weather Review*, *118*(7), 1483–1506. https://doi.org/10.1175/1520-0493(1990)118<1483:AMFCSW>2.0.CO;2

Guiavarch, C., Storkey, D., Blaker, A. T., Blockley, E., Megaan, A., Hewitt, H., et al. (2025). GOSI9: UK Global Ocean and Sea Ice configurations. *Geoscientific Model Development*, *18*(2), 377–403. https://doi.org/10.5194/gmd-18-377-2025

Leister, S. D., Kay, J. E., & Hannay, C. (2025). Local and remote moisture sources both increase late twenty-first century arctic precipitation. *Journal of Climate*, *38*(13), 2963–2973. https://doi.org/10.1175/JCLI-D-24-0359.1

Madec, G., Bourdallé-Badie, R., Chanut, J., Clementi, E., Coward, A., Ethé, C., et al. (2019). NEMO ocean engine. In *Notes du Pôle de modélisation de l'Institut Pierre-Simon Laplace (IPSL)* (Vol. v4.0). https://doi.org/10.5281/zenodo.3878122

McCrystall, M. R., Stroeve, J., Serreze, M., Forbes, B. C., & Screen, J. A. (2021). New climate models reveal faster and larger increases in Arctic precipitation than previously projected. *Nature Communications*, *12*(1), 6765. https://doi.org/10.1038/s41467-021-27031-y

McLaren, A., & Ridley, J. (2026). Supplementary material for the manuscript 'the source of Arctic precipitation in HadGEM3-GC5 [Dataset]. *Zenodo*. https://doi.org/10.5281/zenodo.18611155

McLaren, A. J., Sime, L. C., Wilson, S., Ridley, J., Gao, Q., Gorguner, M., et al. (2025). Implementation of water tracers in the Met Office Unified Model. *Geoscientific Model Development*, *18*(21), 8129–8142. https://doi.org/10.5194/gmd-18-8129-2025

Nusbaumer, J., Wong, T. E., Bardeen, C., & Noone, D. (2017). Evaluating hydrological processes in the Community Atmosphere Model Version 5 (CAM5) using stable isotope ratios of water. *Journal of Advances in Modeling Earth Systems*, *9*(2), 949–977. https://doi.org/10.1002/2016MS000839

Papritz, L., Hauswirth, D., & Hartmuth, K. (2022). Moisture origin, transport pathways, and driving processes of intense wintertime moisture transport into the Arctic. *Weather and Climate Dynamics*, *3*, 1–20. https://doi.org/10.5194/wcd-3-1-2022

Peixoto, J., & Oort, A. (1992). *Physics of climate*. American Institute of Physics.520.

Ridley, J. K., & Blockley, E. W. (2025). Impact of model resolution on the response of Arctic hydrological cycle to climate warming is largely a function of orographic snow. *Climate Dynamics*, *63*(8), 317. https://doi.org/10.1007/s00382-025-07827-0

Ridley, J. K., Blockley, E. W., & Ringer, M. A. (2023). Arctic sea ice causes seasonal differences in the response of Arctic water vapor to climate warming in the CMIP6 model, HadGEM3-GC3.1. *Geophysical Research Letters*, *50*(13), e2022GL102541. https://doi.org/10.1029/2022GL102541

Ridley, J. K., Ringer, M. A., & Sheward, R. M. (2016). The transformation of Arctic clouds with warming. *Climatic Change*, *139*(2), 325–337. https://doi.org/10.1007/s10584-016-1772-4

Rostron, J. W., Bodas-Salcedo, A., Sexton, D. M. H., Jones, C. G., Blockley, E. W., Kuhlbrodt, T., et al. (2026). UKCM2-LL: A new low-resolution GC5 configuration with constrained climate sensitivity – Methodology and development [preprint]. *EGUsphere*. https://doi.org/10.5194/egusphere-2026-1676

Screen, J. A., & Simmonds, I. (2012). Declining summer snowfall in the Arctic: Causes, impacts and feedbacks. *Climate Dynamics*, *38*(11–12), 2243–2256. https://doi.org/10.1007/s00382-011-1105-2

Sellar, A. A., Jones, C. G., Mulcahy, J. P., Tang, Y., Yool, A., Wiltshire, A., et al. (2019). UKESM1: Description and evaluation of the U. K. Earth System Model. *Journal of Advances in Modeling Earth Systems*, *11*(12), 4513–4558. https://doi.org/10.1029/2019MS001739

Singh, H. K. A., Bitz, C. M., Donohoe, A., & Rasch, P. J. (2017). A source-receptor perspective on the polar hydrologic cycle: Sources, seasonality, and Arctic-Antarctic parity in the hydrologic cycle response to CO2 doubling. *Journal of Climate*, *30*(24), 9999–10017. https://doi.org/10.1175/JCLI-D-16-0917.1

Singh, H. K. A., Donohoe, A., Bitz, C. M., Nusbaumer, J., & Noone, D. C. (2016). Greater aerial moisture transport distances with warming amplify inter-basin salinity contrasts. *Geophysical Research Letters*, *43*(16), 8677–8684. https://doi.org/10.1002/2016GL069796

Sundby, S., & Drinkwater, K. (2007). On the mechanisms behind salinity anomaly signals of the northern North Atlantic. *Progress in Oceanography*, *73*(2), 190–202. https://doi.org/10.1016/j.pocean.2007.02.002

Tindall, J. C., Valdes, P. J., & Sime, L. C. (2009). Stable water isotopes in HadCM3: Isotopic signature of El Niño–Southern Oscillation and the tropical amount effect. *Journal of Geophysical Research*, *114*(D4), D04111. https://doi.org/10.1029/2008JD010825

Tsakali, N., Kolbe, M., Bintanja, R., & Skyllas, N. (2025). The time of emergence of Arctic warming, wetting and sea ice melting. *Scientific Reports*, *15*(1), 12626. https://doi.org/10.1038/s41598-025-96607-1

Vancoppenolle, M., Rousset, C., Blockley, E., Aksenov, Y., Feltham, D., Fichefet, T., et al. (2023). SI3, the NEMO Sea Ice Engine (4.2release_doc1.0). *Zenodo*. https://doi.org/10.5281/zenodo.7534900

Vázquez, M., Nieto, R., Drumond, A., & Gimeno, L. (2016). Moisture transport into the Arctic: Source-receptor relationships and the roles of atmospheric circulation and evaporation. *Journal of Geophysical Research: Atmospheres*, *121*(22). https://doi.org/10.1002/2016JD025400

Wang, Z., Ding, Q., Wu, R., Ballinger, T. J., Guan, B., Bozkurt, D., et al. (2024). Role of atmospheric rivers in shaping long term Arctic moisture variability. *Nature Communications*, *15*(1), 5505. https://doi.org/10.1038/s41467-024-49857-y

Willett, M. R., Brooks, M. E., Bushell, A., Earnshaw, P., Marzin, C., Smith, S., et al. (2026). The met office unified model and JULES global atmosphere and land 9.0 configuration [preprint]. *EGUsphere*. https://doi.org/10.5194/egusphere-2026-2425

Wilson, D. R., & Ballard, S. P. (1999). A microphysically based precipitation scheme for the UK meteorological office unified model. *Quarterly Journal of the Royal Meteorological Society*, *125*(557), 1607–1636. https://doi.org/10.1002/qj.49712555707

Wilson, D. R., Bushell, A. C., Kerr-Munslow, A. M., Price, J. D., & Morcrette, C. J. (2008). PC2: A prognostic cloud fraction and condensation scheme. I: Scheme description. *Quarterly Journal of the Royal Meteorological Society*, *134*(637), 2093–2107. https://doi.org/10.1002/qj.333

Wilson, D. R., Bushell, A. C., Kerr-Munslow, A. M., Price, J. D., Morcrette, C. J., & Bodas-Salcedo, A. (2008). PC2: A prognostic cloud fraction and condensation scheme. II: Climate model simulations. *Quarterly Journal of the Royal Meteorological Society*, *134*(637), 2109–2125. https://doi.org/10.1002/qj.332

Xavier, P., Willett, M., Graham, T., Earnshaw, P., Copsey, D., Narayan, N., et al. (2026). Assessment of the Met Office Global Coupled model version 5 (GC5) configurations [preprint]. *EGUsphere*. https://doi.org/10.5194/egusphere-2026-4281

Zapponini, M., & Goessling, H. F. (2024). Atmospheric destabilization leads to Arctic Ocean winter surface wind intensification. *Communications Earth & Environment*, *5*(1), 262. https://doi.org/10.1038/s43247-024-01428-1